Ferroelectric switching of elastin

Yuanming Liu[a,1], Hong-Ling Cai[b,1], Matthew Zelisko[c,d,1], Yunjie Wang[e,f], Jinglan Sun[g], Fei Yan[h], Feiyue Ma[a], Peiqi Wang[a], Qian Nataly Chen[a], Hairong Zheng[h], Xiangjian Meng[g], Pradeep Sharma[c,d], Yanhang Zhang[e,f], and Jiangyu Li[a,2]

[a]Department of Mechanical Engineering, University of Washington, Seattle, WA 98195-2600; [b]National Laboratory of Solid State Microstructures, Department of Physics, Nanjing University, Nanjing 210093, China; Departments of [c]Mechanical Engineering and [d]Physics, University of Houston, TX 77204; Departments of [e]Mechanical Engineering and [f]Biomedical Engineering, Boston University, Boston, MA 02215; [g]National Laboratory for Infrared Physics, Shanghai Institute of Technical Physics, Chinese Academy of Sciences, Shanghai 200083, China; and [h]Paul C. Lauterbur Research Center for Biomedical Imaging, Shenzhen Institutes of Advanced Technology, Chinese Academy of Sciences, Shenzhen 518055, China

Ferroelectricity has long been speculated to have important biological functions, although its very existence in biology has never been firmly established. Here, we present compelling evidence that elastin, the key ECM protein found in connective tissues, is ferroelectric, and we elucidate the molecular mechanism of its switching. Nanoscale piezoresponse force microscopy and macroscopic pyroelectric measurements both show that elastin retains ferroelectricity at 473 K, with polarization on the order of 1 $\mu C/cm^2$, whereas coarse-grained molecular dynamics simulations predict similar polarization with a Curie temperature of 580 K, which is higher than most synthetic molecular ferroelectrics. The polarization of elastin is found to be intrinsic in tropoelastin at the monomer level, analogous to the unit cell level polarization in classical perovskite ferroelectrics, and it switches via thermally activated cooperative rotation of dipoles. Our study sheds light onto a long-standing question on ferroelectric switching in biology and establishes ferroelectricity as an important biophysical property of proteins. This is a critical first step toward resolving its physiological significance and pathological implications.

Ferroelectricity was first discovered in synthetic materials in 1920 when spontaneous polarization of Rochelle salt was found to be switchable by an external electric field (1). Ferroelectrics thus belongs to a larger class of pyroelectric materials that possess a unique polar axis, which, in turn, belongs to piezoelectrics exhibiting linear coupling between electric and mechanical fields (2). Because of these versatile properties, ferroelectric materials are promising for a wide range of technological applications in data storage, sensing, actuation, energy harvesting, and electro-optic devices (3). Biological tissues, such as bones and tendons, were first observed to be piezoelectric in 1950s (4), and shortly thereafter, pyroelectricity was discovered in a variety of biological materials as well (5, 6). Ever since then, ferroelectricity has been speculated for biological systems, and its potential physiological significance has been suggested (7). For example, it was hypothesized that the conformation transition in voltage-gated ion channels is ferroelectric in nature (8, 9). Nevertheless, indication of ferroelectricity in biological materials has only recently emerged from nanoscale piezoresponse force microscopy (PFM) studies (10–13).

This work is motivated by our recent observation of PFM switching in elastin (12), which has generated quite a bit of excitement, although there is still considerable skepticism regarding the notion of biological ferroelectricity. Such reservation is understandable, given the unusual phenomenon of ferroelectric switching in biology, some ambiguities associated with PFM hysteresis, and a current lack of understanding of the basic science underpinning the switching mechanism. Indeed, there is neither macroscopic evidence of ferroelectric switching nor microscopic understanding of its molecular origin. The current work seeks to address these aforementioned issues, and thus to advance our understanding of biological ferroelectricity on two important fronts. First, we present macroscopic observation of ferroelectric switching in a biological system, derived from

careful pyroelectric measurement. This dataset, in our view, decisively settles the long-standing question regarding ferroelectricity in biology. Furthermore, in close conjunction with experiments, we present a molecular-based computational study to elucidate the origin and mechanism underpinning ferroelectric switching of elastin. We show that the polarization in elastin is intrinsic at the monomer level, analogous to the unit cell level polarization in classical perovskite ferroelectrics. Our findings thus establish ferroelectricity as an important biophysical property of proteins, and we believe this is a critical first step toward resolving its physiological significance and pathological implications.

Results and Discussion

Elastin is an ECM protein present in all connective tissues of vertebrates (14), rendering essential elasticity and resilience to aorta, lung, ligament, and skin subjected to repeated physiological stresses (15). Long thought to be purely mechanical, considerable evidence has now emerged regarding its physiological significance (16), for example, in vascular morphogenesis (17, 18) and homeostasis (19) and in regulating cell functions (16). Elastin is also incredibly durable with a $t_{1/2}$ on the order of 70 y, during which it undergoes more than 1 billion cycles of stretching and relaxation (20). Equally remarkable is its durability under high temperature, as found in this study while the sample was heated in searching for a possible ferroelectric phase transition. The elastin was prepared according to a procedure described in *Materials and Methods*, and its fibrous structure is evident from

---

Significance

Ferroelectricity has long been speculated to have important biological functions, although its very existence in biology has never been firmly established. Here, we present, to our knowledge, the first macroscopic observation of ferroelectric switching in a biological system, and we elucidate the origin and mechanism underpinning ferroelectric switching of elastin. It is discovered that the polarization in elastin is intrinsic at the monomer level, analogous to the unit cell level polarization in classical perovskite ferroelectrics. Our findings settle a long-standing question on ferroelectric switching in biology and establish ferroelectricity as an important biophysical property of proteins. We believe this is a critical first step toward resolving its physiological significance and pathological implications.

---

the ultrasonic, histology, scanning probe microscopy (SPM), and transmission electron microscopy (TEM) images shown in *SI Appendix I*, Fig. S1. It possesses a hierarchical microstructure spanning multiple length scales, with tropoelastin monomers cross-linked to form elastin fibers, as shown schematically in *SI Appendix I*, Fig. S1E. The elastic fibers, in turn, form a fiber network. SPM experiments, on the scale of 5 μm, were carried out on elastin fibers. Thermal gravimetric analysis and differential scanning calorimetry (DSC) measurement indicate a weight loss commensurate with the loss of water, suggesting that naturally dried samples retain much of the water and are, in fact, hydrated. Furthermore, elastin survives temperatures as high as 473 K without obvious phase transition or decomposition (*SI Appendix I*, Fig. S2), and a histological image taken at room temperature after elastin was immersed into an oil bath at 473 K for 5 min shows that the fibrous structure of the elastin is intact (Fig. 1A). PFM phase (Fig. 1B) and amplitude (Fig. 1C) mappings confirm the piezoelectricity of elastin at 473 K, from which an interface separating domains of opposite polarity is evident in the phase mapping. More importantly, PFM switching carried out at a series of temperatures results in characteristic hysteresis (Fig. 1D) and butterfly (Fig. 1E) loops with coercivity in the range of 10s V, suggesting that elastin retains its ferroelectric switching at 473 K. In fact, from our modeling, which combines molecular dynamics (MD) simulation and a coarse-grained sta-

tistical mechanics (SM) approach, to be discussed later, the Curie temperature of elastin is found to be 570 K, far above its decomposition temperature. It is much higher than the Curie temperature of any known synthetic molecular ferroelectrics (21), and many oxide ferroelectrics as well, and is comparable to that of lead zirconate titanate, the best-known synthetic ferroelectric.

It is, of course, important to account for possible artifacts in the PFM measurements. First, electrochemical contributions to our PFM data can be excluded. A true electrochemical strain in an SPM experiment arises from the molar volume change associated with different ionic concentrations (22), and such strain would not reverse its phase when the dc bias is reversed, as observed in many electrode materials for lithium ion batteries (22, 23). The electrochemical strain thus cannot be responsible for the switching observed in elastin. In some ionic systems, such as silica glasses, diffusion of ions could result in induced dipole moment, and thus apparent phase switching in PFM upon dc bias (24). However, such hysteresis disappears at a high temperature over 373 K, accompanied by an increased response amplitude, both of which result from faster ionic dynamics with increased temperature (24). The switching in elastin, on the other hand, is retained at temperatures as high as 473 K, and the response amplitude decreases with increased temperature, as in typical ferroelectrics. In fact, elastin samples used for PFM experiments were thoroughly washed, and ionic species or external charges, if any, should be negligible. We can also exclude the effects of silicon substrate, which is coated with gold as the bottom electrode for the sample, and thus is screened from any electric field. In fact, we carried out control experiments on a plastic tape with a gold-coated silicon substrate, which yields no switching characteristics, as shown in *SI Appendix I*, Fig. S3. Because aortic walls are known to be piezoelectric (25), we believe the ferroelectric switching of elastin is indeed intrinsic, as we confirm by MD simulations later. With increasing temperature, it is also observed that the switching asymmetry in elastin is reduced substantially, suggesting thermal activation that reduces the internal asymmetry in its polar structure.

It is worth noting that elastin exhibits PFM switching at room temperature, without the need for prior heating to dehydrate its water content. Nevertheless, the high-temperature PFM studies of elastin suggest that it may be possible to measure its polarization on a macroscopic scale through pyroelectric current, a technique that is much more sensitive than Sawyer tower circuit and can avoid difficulties associated with a large leakage current in porous materials, such as elastin. This allows us to test ferroelectric switching at the macroscopic level to establish the phenomenon firmly, given some ambiguities associated with PFM. To this end, elastin was heated to 480 K first and then electrically poled by applying a 300 V field while it was cooled to room temperature, referred to as positive poling; such poling at an elevated temperature is commonly applied to synthetic ferroelectrics to align their polarization. The sample was then shortened electrically to remove possible space charges and heated again at the rate of 10 K/min, with the pyroelectric current simultaneously measured (Fig. 2A). It is observed that the current increases with rising temperature and reaches 2 nA at 473 K, suggesting that reduced negative polarization with increased temperature results in a positive current. More importantly, when the poling voltage is reversed to −300 V, referred to as negative poling, the pyroelectric current is found to be reversed as well, and the positive and negative currents are approximately symmetrical with respect to each other. In contrast, when collagen was subjected to similar measurements, the current measured is found to be quite noisy and does not seem to reverse under reversed poling (Fig. 2A), suggesting no polarization switching. This is consistent with numerous PFM measurements showing no polarity switching in collagen (26, 27), and it serves as a good control. A question remains, however, on the
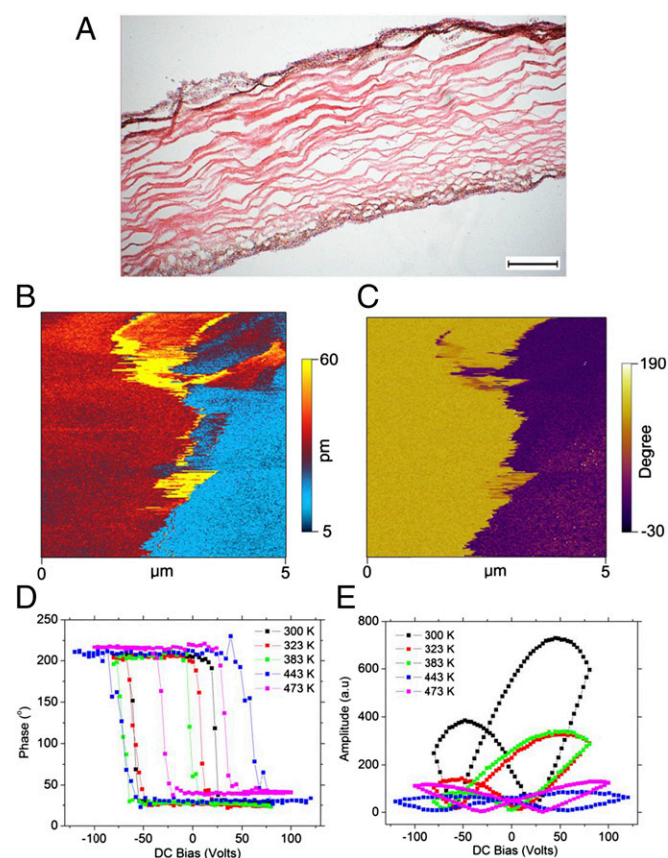

Fig. 1. Ferroelectric properties of elastin at high temperature. (*A*) Histological image taken at room temperature after the sample is immersed into an oil bath at 473 K for 5 min shows that the fibrous structure of elastin is intact. (Scale bar: 200 μm.) Phase (*B*) and amplitude (*C*) mappings of PFM taken at 473 K confirm the high-temperature piezoelectricity of elastin. Hysteresis (*D*) and butterfly (*E*) loops of PFM measured at a series of temperatures show that ferroelectric switching of elastin is preserved at 473 K. a.u. denotes arbitrary unit.
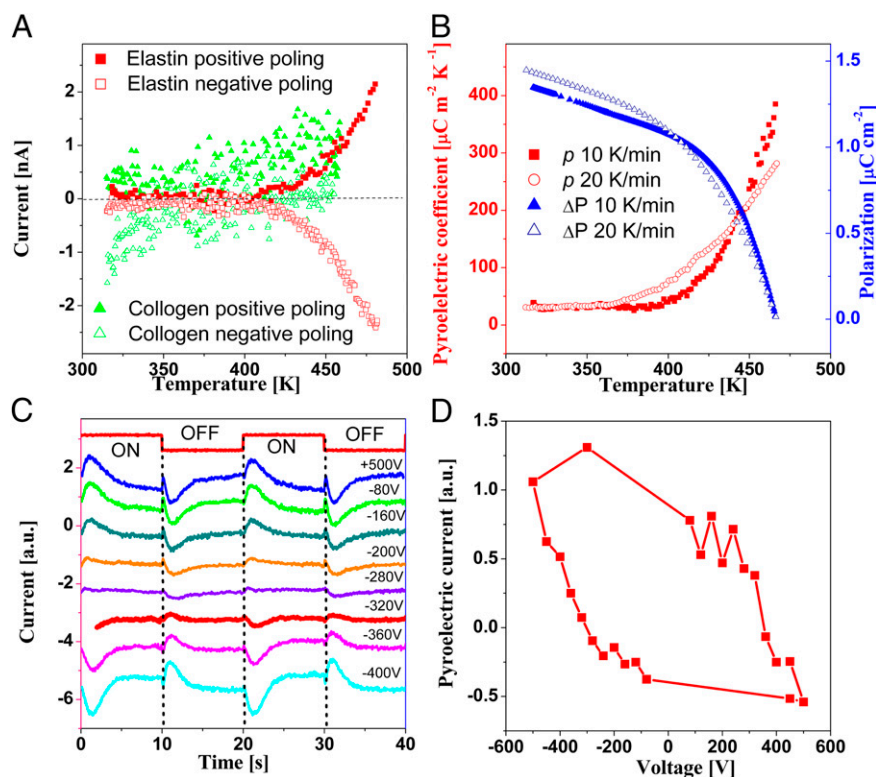
Liu et al.

Fig. 2. Ferroelectric switching of elastin confirmed by pyroelectric measurement. (*A*) Reversed poling voltage switches the pyroelectric current of elastin but not collagen, where positive poling refers to poling by a positive voltage of 300 V and negative poling refers to poling by a negative voltage of −300 V. (*B*) Pyroelectric measurements under different heating rates, revealing consistent pyroelectric coefficients and polarization after integration of the pyroelectric current. (*C*) Pyroelectric current measured at room temperature using the Chynoweth method (28) under different poling voltages, confirming polarization reversal with opposite poling. (*D*) Pyroelectric current as function of poling voltage measured when the pulse laser is turned from on to off, showing a characteristic hysteresis loop.

possible contribution of injected space charges to the measured current; thus, we repeated pyroelectric measurements using a different heating rate, resulting in a different pyroelectric current (*SI Appendix I*, Fig. S4) yet consistent values of polarization (on the order of 1 μC/cm²) and pyroelectric coefficients [on the order of 400 μC/(m²·K)], as shown in Fig. 2*B*. To eliminate the effects of charge injection at a high temperature under large voltage completely, we also poled the sample at room temperature, without prior heating, and then measured the pyroelectric current after removing the poling voltage using the method of Chynoweth (28), by turning a pulse laser on and off to change the sample temperature periodically at room temperature, as shown in Fig. 2*C*. After 500 V poling, a positive pyroelectric current peak is observed when the laser is turned on, which decays to close to zero as the temperature stabilizes. When the laser is turned off, a reversed negative current peak is observed, and the signs of the current peaks reverse between each off/on and on/off transition, corresponding to polarization changes induced by temperature increase and decrease. Notice that the currents measured during heating and cooling cycles are approximately symmetrical to each other, suggesting that thermal-stimulated current is negligible (29). Importantly, as the poling voltage reverses, the magnitude of the current peak gradually reduces, and the sign eventually reverses at around −320 V, after which the current increases with increased poling voltage, suggesting polarization switching at around −320 V. A similar reversal is also observed when we started with poling at −500 V, as shown in *SI Appendix I*, Fig. S5. By plotting the peak pyroelectric current at the on/off transition against the poling voltage over one complete cycle of poling voltages, a characteristic hysteresis loop is obtained (Fig. 2*D*), and this firmly estab-

lishes macroscopic ferroelectric switching in elastin. More details of such measurements, especially on eliminating the contributions from nonpyroelectric sources, are discussed in *SI Appendix I*. In particular, the Chynoweth technique (28) is effective in reducing the effect of trapped charges, because the sample remains at an essentially constant average temperature, leading to relatively rapid depletion of the trapped charge available for release at that temperature (29). In addition, the magnitude of any thermal-stimulated current will be markedly different when induced in response to cooling and heating, and this would result in a highly asymmetrical waveform of current (29). The good symmetry of our measured current during heating and cooling cycles indicates that the effects of thermal-stimulated charges can be largely excluded and that the current we measured in elastin is indeed pyroelectric in nature.

Elastin is composed of cross-linked tropoelastin monomers, and the properties of elastin are expected to be retained across different length scales down to tropoelastin (30–32). To understand the mechanism of polarization and ferroelectric switching in elastin, we carried out an MD simulation of tropoelastin monomer. In an attempt to mimic the biological system as closely as possible, the entire 792-aa sequence found in natural human elastin is computed instead of the recombinant 698-aa sequence commonly used in tropoelastin experiments, corresponding to around 10,000 atoms (33). The 698-aa protein has also been simulated, and the difference between the two models is negligible. To date, the structure of tropoelastin has not been fully characterized experimentally, and the best estimates so far only provide an overall shape of the monomer with no information on folding patterns or the secondary structure (31). As such, we adopted a protein threading approach, also called fold recognition,

which uses the amino acid sequence to place each amino acid in the best-fit position based on other folds commonly found in nature. The initial structure created for tropoelastin by this method is fairly close to the expected general structure (34). Energy minimization was then performed on the folded structure, after which an MD simulation was performed at 300 K for 1,000 ps to equilibrate the system. The protein reaches a stable folded configuration (Fig. 3A and *SI Appendix I*, Fig. S6) in good agreement with the experimentally observed shape of tropoelastin, and its end-to-end length of 12.2 nm is also close to the 16-nm value reported experimentally (31). A second MD simulation was then performed on the equilibrated structure for 200 ps, from which the time-averaged dipole moment of tropoelastin monomer is calculated to be 801 ± 41 Debye. This indicates that the polarization of elastin is intrinsic at the monomer level, analogous to the unit cell level polarization in perovskite ferroelectrics. With the molecular volume estimated to be 107 nm^2 from the MD simulation, the maximum spontaneous polarization of elastin, when all of the monomers are aligned, is estimated from the dipole moment per unit molecular volume as 2.25 μC/cm^2, which is in reasonable agreement with experimental values integrated from the pyroelectric current.

It is well known that tropoelastin monomers are regularly cross-linked in elastic fibers (30–32), which are aligned to a certain extent as well (Fig. 1A and *SI Appendix I*, Fig. S1). To study the collective behavior of such an array of dipolar tropoelastin monomers, a simple SM model originally developed for PVDF was adopted (35), with which the ferroelectricity of elastin can be studied. In the absence of an external electric field, two equivalent wells in a free-energy landscape corresponding to two opposite polarization directions are observed (Fig. 3B); however, with an external electric field applied, one of the wells becomes gradually disfavored, resulting in eventual alignment of all dipole moments beyond the critical coercive field. When the external electric field is reversed in direction, a polarization hysteresis loop results (Fig. 3C), which is in good agreement with the PFM hysteresis recorded on tropoelastin and will be discussed next. Furthermore, an order–disorder transition is found to occur at a Curie temperature of 580 K, consistent with experimental observation of ferroelectricity at 473 K. The process of polarization switching can be understood from a structure model of elastin recently proposed (31), consisting of a tropoelastin monomer chain connected in head-to-tail manner (Fig. 3D), wherein the dipole moment is approximately normal to the chain axis. Although this model is speculative, it reflects a certain degree of supermolecular ordering exhibited in microscopic images (*SI Appendix I*, Fig. S1), and it is consistent with the macroscopic polarization we observed in elastin, resulting from the collective effect of aligned dipolar tropoelastin monomers. When an electric field perpendicular to the chain axis yet opposite to the dipole moment is applied, MD simulations suggest that tropoelastin monomers will reconfigure until the dipole moment is aligned with the electric field (*SI Appendix I*, Fig. S7), resulting in polarization reversal. Such rotation, however, would be considerably slower than ionic displacement in perovskite ferroelectrics.

Our coarse-grained MD simulations capture several of the key features of tropoelastin structure that are experimentally known, and the overall model correctly predicts the polarization reversal that underpins ferroelectricity in elastin. The ferroelectric switching of tropoelastin monomers was indeed verified by PFM measurements, with the PFM response vs. voltage curve showing bilinear characteristics (Fig. 4A). The transition occurs at ~7 V, presumably due to a poling-enhanced piezoelectric response at higher voltage, because the tropoelastin powders were randomly distributed
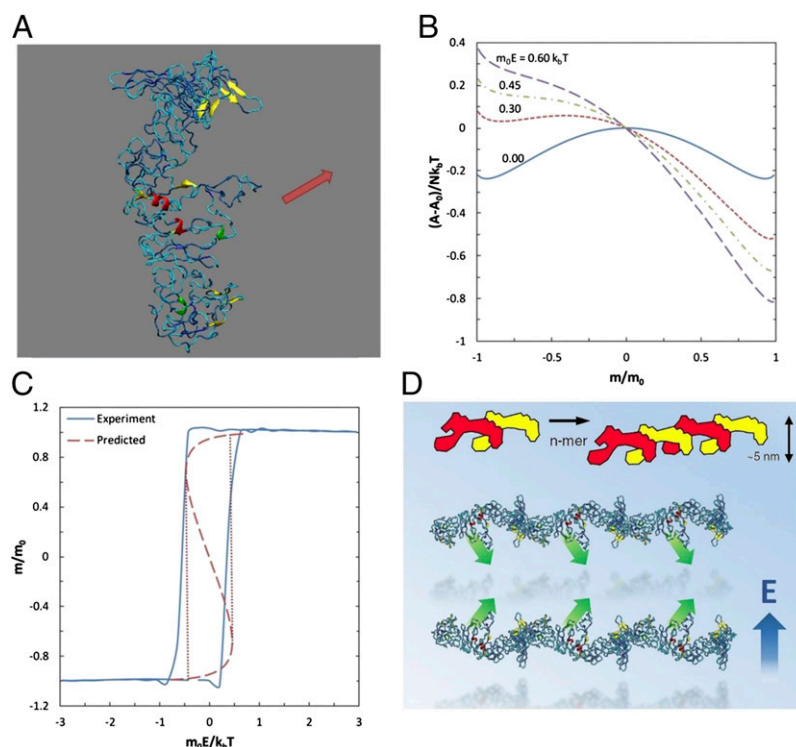

Fig. 3. Molecular mechanism of ferroelectricity of elastin. (A) Equilibrated molecular structure of tropoelastin, with polar direction identified by the arrow. (B) Free-energy landscape of the tropoelastin lattice as a function of polarization m, where m_0 is the total dipole moment per unit volume in the system, N is the total number of dipoles, k_b is the Boltzmann constant, and T is the absolute temperature. (C) Hysteresis loops predicted from SM simulations and measured by PFM. (D) Schematics of the heat-tail configuration of tropoelastin monomers proposed in a study by Yang et al. (34) and the envisioned molecular structure with a dipole moment that can be rotated by the applied electric field.

initially. The mappings of the vertical PFM phase (Fig. 4B) and amplitude (Fig. 4C) over a 0.5×0.5-μm^2 area show good piezo-electricity of tropoelastin, and the corresponding lateral PFM mappings are shown in *SI Appendix I, Fig. S8*. The switching spectroscopy PFM mapping carried out on 8×8-grid points over a 6×6-μm^2 area reveals consistent ferroelectric switching (Fig. 4D), although the distributions are not uniform, and the heterogeneity arises from random distribution of the highly anisotropic tropoelastic monomers. Characteristic hysteresis (Fig. 4E) and butterfly (Fig. 4F) loops at three representative points are given, showing quite different PFM responses at zero voltage, yet the coercive voltage is very uniform (*SI Appendix I, Fig. S8*), less than 10 V, similar to what we observed in aortic walls and elastin (11, 12), and is consistent with the kink point seen in Fig. 4A. The hysteresis loops predicted by MD/SM and measured by PFM agree well with each other (Fig. 3C), confirming the molecular mechanism of ferroelectric switching as revealed by MD simulations.

What we learned from this set of experimental and computational studies is quite revealing. Classical ferroelectricity is defined for a crystalline system, with spontaneous polarization well defined at the unit cell level. The elastin, although not crystalline, possesses strong polarization at the monomer level; thus, a certain degree of supermolecular ordering, as seen from the microscopic images in *SI Appendix I, Fig. S1* and the proposed structure model in Fig. 3D, leads to macroscopic polarization and its switching. In other words, the polarization is intrinsic to the molecular structure of elastin, analogous to ferroelectric perovskite, wherein the polarization is built in the unit cell. This is markedly different from electrets or electrochemical systems wherein the polarizations are extrinsic, induced by either injected charges or ionic activities. As discussed earlier, we have excluded the effects of trapped charges from our pyroelectric measurements, and electrochemical contributions to our PFM measurements are negligible as well. The polarization thus is intrinsic to elastin.

In summary, we have confirmed ferroelectricity in a biological system at the macroscopic scale and uncovered the molecular mechanism of its switching. There are a number of points worth noting. First, elastin has quite remarkable ferroelectric properties compared with synthetic molecular ferroelectrics. It has the highest Curie temperature and maintains its integrity and

ferroelectricity at 473 K, and its spontaneous polarization on the order of 1 $\mu C/cm^2$ is one of the highest among molecular systems. Although the voltage necessary to switch the macroscopic sample is relatively high due to the large thickness, the local switching at the nanometer scale, as revealed by the PFM, is much smaller. Although people are still striving to develop synthetic molecular systems with good ferroelectric properties (21), nature seems have mastered the effect for millions of years, and this could shed light onto developing new synthetic molecular ferroelectrics with improved performances. Second, although elastin is ferroelectric, collagen, a much more ancient and ubiquitous protein in biology, appears to be nonswitchable, pointing toward the possibility of nature selection during evolution (19). Indeed, elastin is only found in arteries of vertebrates (19), as well as in the later stage of embryonic development (36), wherein blood pressure is notably higher. This leads to our key puzzle: Is ferroelectricity of elastin just coincidental in biology, or does it actually serve important physiological functions? This is an open question remaining to be answered, yet there are a number of possible implications. For example, ferroelectric switching may help damp out the increased pulsatile flow and blood pressure in arteries to reduce distal shear stress. The polarization in elastin may also help in regulating proliferation and organization of vascular smooth muscle and contribute to arterial morphogenesis (17). Furthermore, it was recently reported that ferroelectric switching in elastin is suppressed by glucose (12); thus, there could be a connection between loss of ferroelectricity and aging, during which glycation naturally occurs (37, 38). Our study settles a long-standing question on the existence of ferroelectricity in biological systems, yet this is just a first step toward resolving its physiological significance and pathological implications.

Materials and Methods

Elastin and Collagen. Porcine thoracic aortas were harvested from a local abattoir and transported to the laboratory on ice. The aortas were cleaned of adherent tissues and fat and rinsed in distilled water. Samples were cut into squares of about 20×20 mm^2 from the cleaned aortas. All samples were taken from a similar longitudinal region of aortas to minimize the changes of properties with a longitudinal position. Elastin samples were obtained using cyanogen bromide (CNBr; Acros Organics) treatment to remove cells, collagen, and other ECM components. Briefly, fresh aortic samples were treated with 50 mg/mL CNBr in 70% (vol/vol) formic acid solution for 19 h at
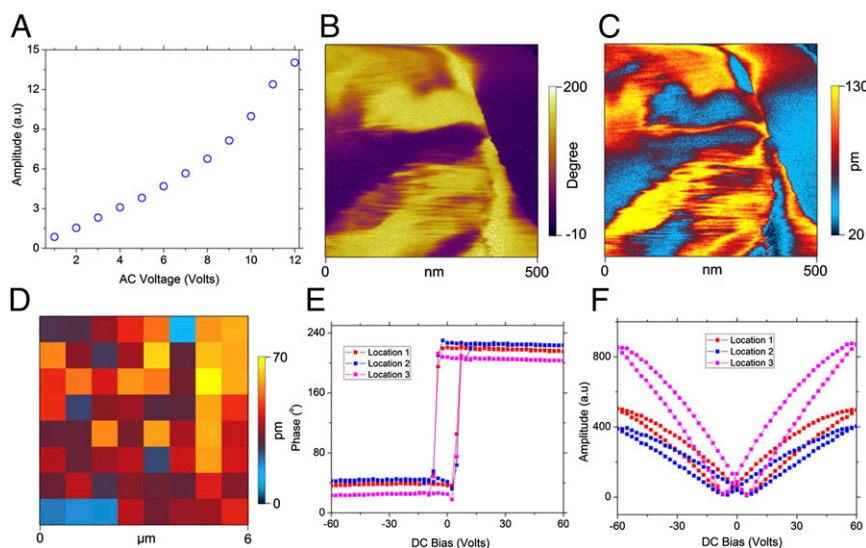

Fig. 4. Ferroelectricity of tropoelastin monomers. (A) PFM response vs. ac voltage shows bilinear characteristics. Phase (B) and amplitude (C) mappings of PFM. (D) Switching spectroscopy PFM mapping of the PFM response at zero dc voltage shows consistent switching. Hysteresis (E) and butterfly (F) loops of three representative points.

room temperature and for 1 h at 60 °C with gentle stirring, followed by 5 min of boiling to inactivate CNBr. Collagen samples were obtained by treating aortic samples with 5 U/mL ultrapure elastase (MP Biomedicals, LLC), 1 mM $CaCl_2$, and 0.02% NaN_3 in 100 mM Tris buffer at 37 °C with gentle stirring for 4 d. All samples were rinsed thoroughly and kept in 1× PBS solution for further experiments. To prepare for PFM experiments, samples were fixed with 4% paraformaldehyde in PBS for 1 h at room temperature. The fixed samples were washed in a graded distilled water/ethanol series [30%, 50%, 70%, and 100% (vol/vol) for 15 min each], followed by washes with a graded ethanol/hexamethyldisilazane series [30%, 50%, 70%, and 100% (vol/vol) for 15 min each], and finally allowed to dry overnight. Each section was then split into two halves in the cross-section, cut into 8×8-mm^2 pieces, and glued on silicon substrate sputtered with 100-nm thick gold using silver paint for PFM studies.

Tropoelastin. A tropoelastin sample derived from recombinant processing methods was purchased from Advanced BioMatrix and supplied as a sterile, lyophilized powder. In preparation for PFM, tropoelastin powder was first pressed into a small sheet by glass slides with a thickness of ∼300 μm. The tropoelastin sheet was then glued on silicon substrate sputtered with 100-nm thick gold using silver paint and dried in the freezer (∼0 °C) for over 5 h before PFM studies.

H&E Staining. To prepare for microscopic examination, the elastin samples were covered with Tissue-Tek (Sakura) and then frozen in liquid nitrogen vapor. The elastin sections (5-μm thick) were cut with a cryostat microtome (CM1950; Leica). A microscope slide was used for bearing cryosections and immersing the slide in H_2O for 30 s with agitation by hand, followed by dipping the slide into a Coplin jar containing Mayer's hematoxylin for 30 s. The slide was then rinsed in H_2O for 1 min. After that, the slide was stained with 1% eosin Y solution for 10–30 s with agitation. After the sections were dehydrated with two changes of 95% alcohol and two changes of 100% alcohol (each change for 30 s), one drop of mounting medium was added and covered with a coverslip. Elastin sections were viewed under a light microscope (Olympus BX43 microscope).

Ultrasonic Imaging. To prepare for ultrasound imaging, the dried elastin samples were cut into pieces of about 10×5 mm^2. These samples were kept in 1× PBS solution and vacuum pumped for 1 h. The elastin samples were then fixed by two threads (each for one terminal) in a transparent tank, which was filled with degassed PBS. The transducer was fixed on a railing system to maintain the acoustic focus at the center of the samples. Ultrasonic imaging was performed in B-mode using a Vevo2100 high-frequency ultrasound system (VisualSonics, Inc.), which was equipped with a 40-MHz center frequency transducer. All imaging parameters (focal length, 5 mm; gain, 10 dB; transmit power, 100%; dynamic range, 35 dB) were kept constant during all imaging sessions.

TEM. To prepare for TEM, the fresh elastin samples were fixed in Karnovsky's fixative for 2 h, followed by 2% OsO_4 in buffer for 2 h. After ethanol dehydration, the samples were infiltrated in 2 mL of propylene oxide and 2 mL of resin solution for 1 h. The drained tissues were embedded in fresh resin and then trimmed with a saw. Sections were mounted on a TEM grid and allowed to dry overnight. Finally, the sections were stained with 2% uranyl acetate (aqueous) for 5 min. The fibrous structure of elastin was examined by TEM using an FEI Tecnai G2 F20 microscope operated at 200 kV.

SPM. An Asylum Research MPF-3D atomic force microscope was used for SPM and PFM studies. The probe was made of silicon, with the lever coated with aluminum and the tip coated with titanium/iridium (3:15), and the radius of tip was 23 ± 10 nm. The resonance frequency of the lever in air was 73 kHz, and the spring constant of the lever was 2 N/m. During the switching PFM, two cycles of dc bias were applied, starting from zero toward the positive voltage, with the period set to be 5 s and each "on" and "off" step maintained for 50 ms. All of the data reported in this paper were obtained in the second cycle.

Thermogravimetric Analysis and DSC. A small piece of the dehydrated elastin sample (8.382 mg) was utilized for thermogravimetric analysis using a TGA7 thermogravimetric analyzer (PerkinElmer). The sample was first heated up to 40 °C from room temperature and kept for 15 min, and it was then ramped to 400 °C with a heating rate of 5 °C/min. DSC using the dehydrated elastin sample was carried out using a Q20 differential scanning calorimeter (TA Instruments). A heat/cool/heat profile from 30 °C to 250 °C was used for the measurement to eliminate the water residue and thermal history. The heating and cooling rates were both 10 °C/min, and 5-min isothermal stages were used between heating and cooling sections.

Pyroelectric Measurement. For the high-temperature experiment, silver conduction paste was deposited on the sample surfaces as electrodes for pyroelectric measurement using a Keithley 6517B electrometer (Keithley Instruments, Inc.). The elastin sample was cooled down from about 480 K to room temperature with a positive or negative 300 V electric field applied. The electric field was then removed, and the pyroelectric current was measured in a heating process with a constant heating rate. The hysteresis curve of the pyroelectric current was obtained utilizing the Chynoweth technique (28) at room temperature, using samples without prior heating treatment. The electrodes of the sample were prepared by evaporating gold onto both sides of the sample. The sample, with a thickness of 100 μm and an area of 4 mm^2, was suspended within a sample holder and thermally isolated from the environment via two aluminum bonding wires that also served as electrodes. The temperature of the sample was changed periodically by a pulsed laser with wavelength of 1.47 μm and power of 100 mW modulated at a low frequency of 50 mHz. The pyroelectric current was measured using a Keithley 6517a electrometer (Keithley Instruments, Inc.) and amplified further with a SR560 low-noise voltage preamplifier (Stanford Research Systems).

MD Simulation and Statistical Model. Details on the MD simulation and statistical model are presented in *SI Appendix II*.

1. Valasek J (1921) Piezo-electric and allied phenomena in Rochelle salt. *Phys Rev* 17(4): 475–481.
2. Lines EM, Glass AM (1977) *Principles and Applications of Ferroelectrics and Related Materials* (Oxford Univ Press, New York).
3. Scott JF (2007) Applications of modern ferroelectrics. *Science* 315(5814):954–959.
4. Fukada E, Yasuda I (1957) On the piezoelectric effect of bone. *J Phys Soc Jpn* 12(10): 1158–1162.
5. Lang SB (1966) Pyroelectric effect in bone and tendon. *Nature* 212:704–705.
6. Athenstaedt H, Claussen H, Schaper D (1982) Epidermis of human skin: Pyroelectric and piezoelectric sensor layer. *Science* 216(4549):1018–1020.
7. Lang SB (2000) Piezoelectricity, pyroelectricity and ferroelectricity in biomaterials— Speculation on their biological significance. *IEEE Trans Dielectr Electr Insul* 7(4): 466–473.
8. Leuchtag HR (1987) Indications of the existence of ferroelectric units in excitable-membrane channels. *J Theor Biol* 127(3):321–340.
9. Leuchtag HR, Bystrov VS (1999) Theoretical models of conformational transitions and ion conduction in voltage-dependent ion channels: Bioferroelectricity and superionic conduction. *Ferroelectrics* 220(1):157–204.
10. Li T, Zeng K (2011) Piezoelectric properties and surface potential of green abalone shell studied by scanning probe microscopy techniques. *Acta Mater* 59(9):3667–3679.
11. Liu Y, Zhang Y, Chow MJ, Chen QN, Li J (2012) Biological ferroelectricity uncovered in aortic walls by piezoresponse force microscopy. *Phys Rev Lett* 108(7):078103.
12. Liu Y, et al. (2013) Glucose suppresses biological ferroelectricity in aortic elastin. *Phys Rev Lett* 110(16):168101.
13. Heredia A, et al. (2012) Nanoscale ferroelectricity in crystalline gamma-glycine. *Adv Funct Mater* 22(14):2996–3003.
14. Pasqualironchetti I, Baccaranicontri M, Fornieri C, Mori G, Quaglino D (1993) Structure and composition of the elastin fiber in normal and pathological conditions. *Micron* 24(1): 75–89.
15. Daamen WF, Veerkamp JH, van Hest JCM, van Kuppevelt TH (2007) Elastin as a biomaterial for tissue engineering. *Biomaterials* 28(30):4378–4398.
16. Debelle L, Tamburro AM (1999) Elastin: Molecular description and function. *Int J Biochem Cell Biol* 31(2):261–272.
17. Li DY, et al. (1998) Elastin is an essential determinant of arterial morphogenesis. *Nature* 393(6682):276–280.
18. Brooke BS, Bayes-Genis A, Li DY (2003) New insights into elastin and vascular disease. *Trends Cardiovasc Med* 13(5):176–181.

19. Faury G (2001) Function-structure relationship of elastic arteries in evolution: From microfibrils to elastin and elastic fibres. *Pathol Biol (Paris)* 49(4):310–325.
20. Li B, Daggett V (2002) Molecular basis for the extensibility of elastin. *J Muscle Res Cell Motil* 23(5-6):561–573.
21. Li J, Liu Y, Zhang Y, Cai H-L, Xiong R-G (2013) Molecular ferroelectrics: Where electronics meet biology. *Phys Chem Chem Phys* 15(48):20786–20796.
22. Jesse S, et al. (2012) Electrochemical strain microscopy: Probing ionic and electrochemical phenomena in solids at the nanometer level. *MRS Bull* 37(7):651–658.
23. Chen NQ, et al. (2012) Delineating local electromigration for nanoscale probing of lithium ion intercalation and extraction by electrochemical strain microscopy. *Appl Phys Lett* 101(6):063901.
24. Proksch R (2014) Electrochemical strain microscopy of silica glasses. *J Appl Phys*, in press.
25. Fukada E, Hara K (1969) Piezoelectric effect in blood vessel walls. *J Phys Soc Jpn* 26(3):777–780.
26. Kalinin SV, Rodriguez BJ, Jesse S, Thundat T, Gruverman A (2005) Electromechanical imaging of biological systems with sub-10 nm resolution. *Appl Phys Lett* 87(5):053901.
27. Rodriguez BJ, et al. (2006) Electromechanical imaging of biomaterials by scanning probe microscopy. *J Struct Biol* 153(2):151–159.
28. Chynoweth AG (1956) Dynamic method for measuring the pyroelectric effect with special reference to Barium Titanate. *J Appl Phys* 27(1):78–84.
29. Lubomirsky I, Stafsudd O (2012) Invited review article: Practical guide for pyroelectric measurements. *Rev Sci Instrum* 83(5):051101–051101.
30. Wise SG, et al. (2014) Tropoelastin: A versatile, bioactive assembly module. *Acta Biomater* 10(4):1532–1541.
31. Baldock C, et al. (2011) Shape of tropoelastin, the highly extensible protein that controls human tissue elasticity. *Proc Natl Acad Sci USA* 108(11):4322–4327.
32. Mithieux SM, Wise SG, Weiss AS (2013) Tropoelastin—A multifaceted naturally smart material. *Adv Drug Deliv Rev* 65(4):421–428.
33. Ostuni A, Bochicchio B, Armentano MF, Bisaccia F, Tamburro AM (2007) Molecular and supramolecular structural studies on human tropoelastin sequences. *Biophys J* 93(10):3640–3651.
34. Yang Y, Faraggi E, Zhao H, Zhou Y (2011) Improving protein fold recognition and template-based modeling by employing probabilistic-based matching between predicted one-dimensional structural properties of query and corresponding native properties of templates. *Bioinformatics* 27(15):2076–2082.
35. Broadhurst MG, Davis GT (1981) Ferroelectric polarization in polymers. *Ferroelectrics* 32(1):177–180.
36. Wagenseil JE, et al. (2010) The importance of elastin to aortic development in mice. *Am J Physiol Heart Circ Physiol* 299(2):H257–H264.
37. Bailey AJ (2001) Molecular mechanisms of ageing in connective tissues. *Mech Ageing Dev* 122(7):735–755.
38. Konova E, Baydanoff S, Atanasova M, Velkova A (2004) Age-related changes in the glycation of human aortic elastin. *Exp Gerontol* 39(2):249–254.